MATERIALS SCIENCE

Size- and composition-controlled intermetallic nanocrystals via amalgamation seeded growth

Jasper Clarysse, Annina Moser, Olesya Yarema, Vanessa Wood, Maksym Yarema*

Intermetallic nanocrystals are a large family of emerging materials with extensive applications in many fields. Yet, a generalized synthetic method for intermetallic nanocrystals is lacking. Here, we report the development of a colloidal synthesis method based on amalgamation of monometallic nanocrystal seeds with low–melting point metals. We use this approach to achieve crystalline and compositionally uniform intermetallic nanocrystals of Au-Ga, Ag-Ga, Cu-Ga, Ni-Ga, Pd-Ga, Pd-In, and Pd-Zn compounds. We demonstrate both compositional tunability across the phase spaces (e.g., $AuGa_2$, AuGa, Au_7Ga_2, and Ga-doped Au), size tunability (e.g., 14.0-, 7.6-, and 3.8-nm $AuGa_2$), and size uniformity (e.g., 5.4% size deviations). This approach makes it possible to systematically achieve size- and composition-controlled intermetallic nanocrystals, opening up a multitude of possibilities for these materials.

INTRODUCTION

Nanocrystals (NCs) of intermetallic compounds (IMCs; long-range ordered alloys) are a vast realm of emerging materials. They offer attractive characteristics originating from well-defined crystallinity, synergistically combined properties of the incorporated metals, and unique size- and surface-related physical and chemical phenomena exhibited by NCs (*1*). Intermetallic NCs have recently acquired a large amount of research interest because of their extensive applications in catalysis (*2*–*5*), electronics, e.g., thermoelectric devices and memory technologies (*6*–*8*), superconductivity (*9*), energy storage and conversion technologies (*10*–*12*), photonics (*13*), and life sciences and medicine (*14*). Remarkable examples of tunable plasmonics (*13*), high-density magnetization (*15*), and outstanding catalytic selectivity (*2*, *16*–*18*) illustrate the great potential for IMC NCs. Nevertheless, a universal synthetic method toward IMC NCs does not yet exist. This is, in part, due to challenges such as the different reduction potentials between metals and metal oxophilicity. Thermal annealing approaches deal with these challenges by stabilizing precursors, for example, on supports (*3*, *19*), in carbon-nitride networks (*20*, *21*), or in molten salts (*22*). In contrast, wet-chemical colloidal synthesis procedures offer tremendous versatility with regard to reagents, ligands, and reaction parameters, yielding dispersions of NCs that are easy to handle and process (*23*), and are therefore an attractive methodology to explore for the synthesis of IMC NCs.

Here, we report the development of a synthesis method to achieve IMC NCs, based on controlled amalgamation of low–melting point metals into monometallic seeds (Fig.1A). We recognize a seeded growth approach as a promising route for incorporating metals with differing reduction potentials in NCs during colloidal synthesis (*24*–*28*). Amalgamation refers to the process of alloying a metal with another low–melting point metal through interdissolution and can be traced back for many millennia from the usage of dental amalgams and the extraction of precious metals from ores (*29*). Combining seed-assisted colloidal synthesis with controlled nanoscale amalgamation gives access to a large family of monodisperse IMC NCs (Fig. 1 and figs. S1 to S3). We highlight the generality of our amalgamation seeded growth synthesis in two ways. First, we amalgamate different metal seeds (Au, Ag, Cu, Pd, and Ni) with Ga to obtain high-quality IMC NCs. Second, we show that, in addition to Ga, other low–melting point metals (In and Zn) can be used. We demonstrate that both the size and size dispersion characteristics of the initial metal NC seeds remain preserved upon amalgamation, thus allowing the synthesis of size-uniform (as small as 5.4% size deviations) and size-tunable intermetallic colloids. Simultaneously, we can control the composition of bimetallic NCs simply by varying the introduced amount of amalgamating metal precursor.

Institute for Electronics, Department of Information Technology and Electrical Engineering, ETH Zurich, Gloriastrasse 35, 8092 Zurich, Switzerland.
*Corresponding author. Email: yaremam@ethz.ch

RESULTS

Amalgamation seeded growth synthesis

The amalgamation seeded growth synthesis is based on the controlled amalgamation of metal seeds with low–melting point metals. It involves the colloidal synthesis of monometallic NCs according to a well-established protocol, followed by the injection of an amalgamating metal and annealing (10 min, $T > 260$ °C; Fig.1A). For amalgamation, metal amides and silylamides are preferred as precursors because of their fast thermal decomposition via cleavage of reactive metal-nitrogen bonds and their previous success in the synthesis of NCs (*30*). Furthermore, high reaction temperatures and the use of mildly reducing aprotic L-type ligands (e.g., oleylamine) (*31*, *32*) enable the synthesis of even very challenging bimetallic compositions in terms of difference in reactivity and reduction potential between the incorporated metals (e.g., Au-Ga NCs; Fig. 1E). The obtained intermetallic NCs are monodisperse (table S1) and compositionally uniform, as is demonstrated with transmission electron microscopy (TEM) images and scanning TEM energy-dispersive x-ray spectroscopy (STEM EDX) elemental maps (Fig.1, B to H). Line scans of STEM EDX maps (Fig. 1, E and G) reveal homogeneous distributions of elements inside the IMC NCs. Moreover, because of the used reaction temperatures, IMC NCs feature high crystallinity, as is reflected in powder x-ray diffraction (XRD) patterns and high-resolution TEM (HRTEM) images (fig. S3). For Ni_2Ga_3 composition, NCs contain voids (fig. S4), originating from a nanoscale Kirkendall effect (*27*, *33*, *34*). Last, a thin amorphous oxide shell (1 to 2 nm) is created upon air exposure (fig. S5), rendering the colloids stable under ambient conditions for many months.

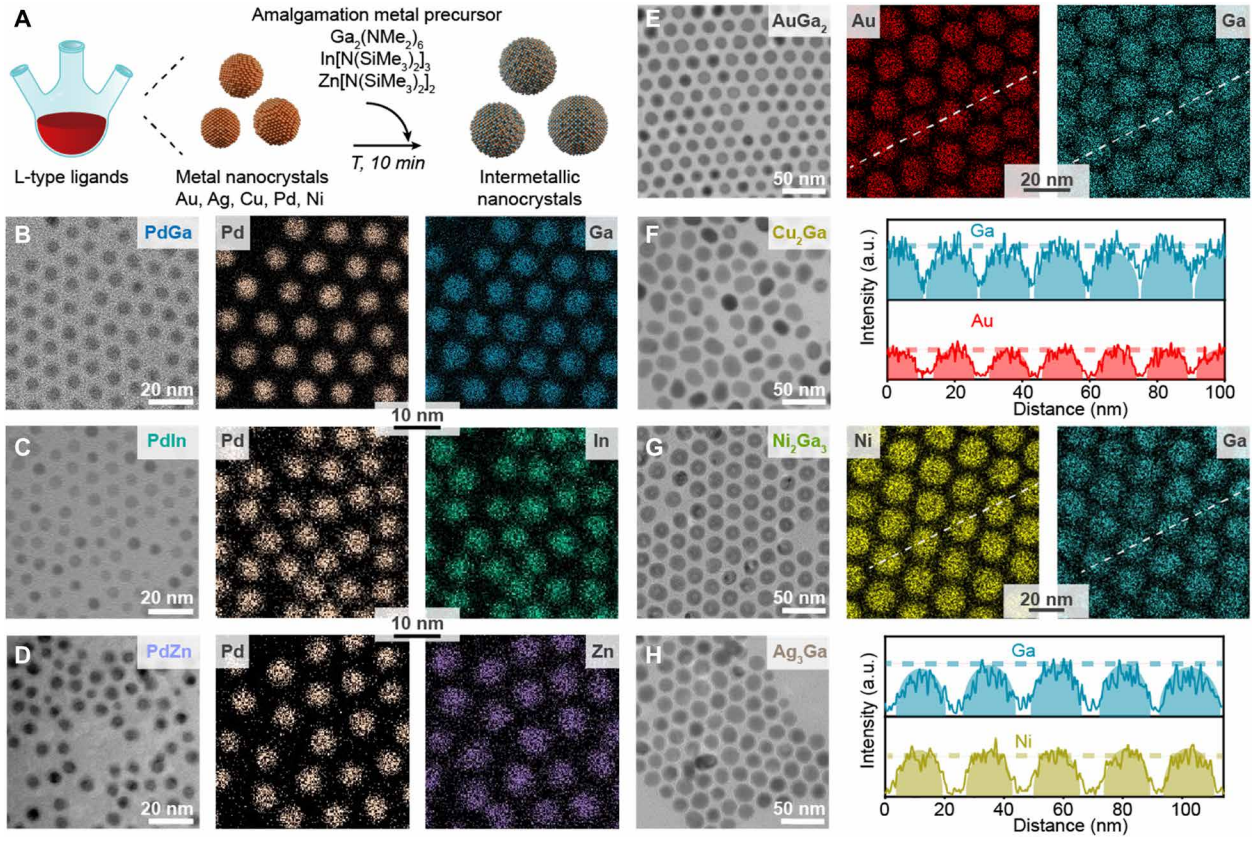

Fig. 1. Amalgamation seeded growth synthesis. (**A**) Schematic illustration of the amalgamation reaction, converting monometallic seeds into intermetallic NCs. As-synthesized PdGa, PdIn, PdZn, $AuGa_2$, Cu_2Ga, Ni_2Ga_3, and Ag_3Ga IMC NCs are shown in TEM images (**B** to **H**) and STEM EDX mappings (B to E and G). Line profile scans for $AuGa_2$ and Ni_2Ga_3 NCs (E and G) highlight the compositional uniformity of the IMC NCs. a.u., arbitrary units.

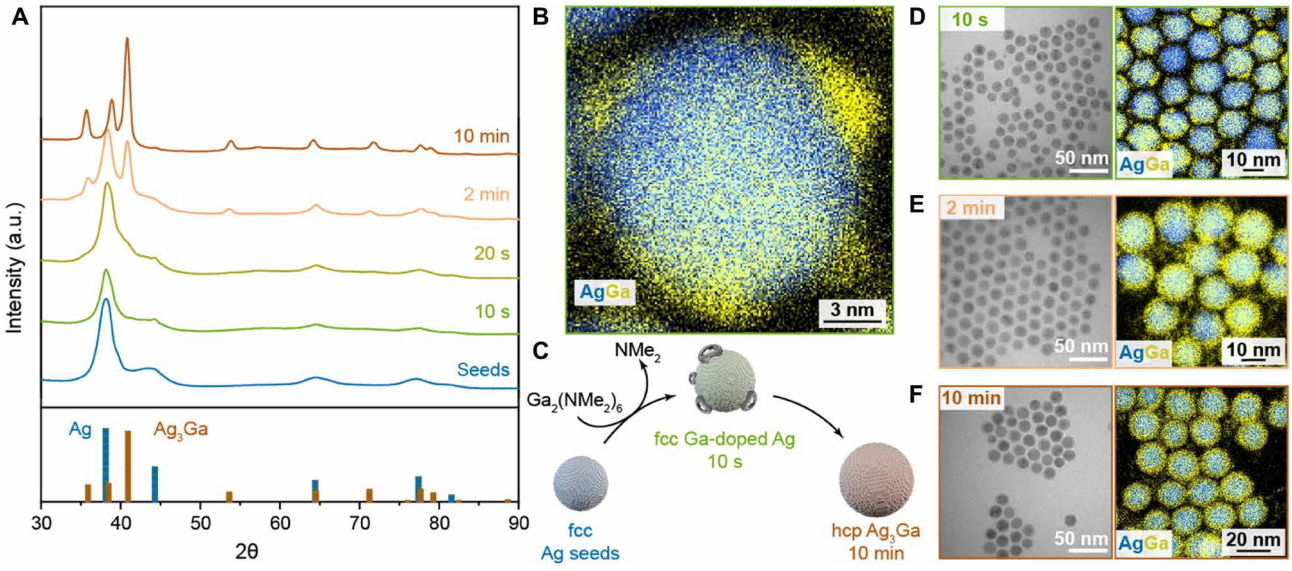

Fig. 2. Amalgamation mechanism. (**A**) XRD patterns measured from aliquots taken during the synthesis of Ag_3Ga NCs reveal the gradual conversion of Ag seeds to the intermetallic phase. Ga shows surface wetting and island growth behavior before intermetallic phase conversion as seen from a STEM EDX map of an aliquot taken after 10 s of reaction time (**B**) and as illustrated in amalgamation schematics (**C**). (**D** to **F**) Aliquots taken after 10 s, 2 min, and 10 min of reaction time are shown in TEM and STEM EDX images.

Amalgamation mechanism

To gain insights into the amalgamation mechanism, we focus on the synthesis of Ag_3Ga NCs. We observe fast doping of Ag seeds by Ga ($t < 10$ s), followed by a gradual conversion to the intermetallic Ag_3Ga phase (Fig. 2). We interpret that the Ga-amide precursor undergoes thermolysis (Fig. 2, B and C), leading to the accumulation of liquid Ga on the NC surface without epitaxial constraints (*35*–*37*). Quick doping kinetics can be attributed to the fast thermolysis of the Ga-amide precursor and the large diffusion coefficient of liquid Ga (*38*), combined with the fact that Ga-doped Ag is a solid solution within the face-centered cubic (fcc) Ag phase. By 2 min of reaction time (Fig. 2E and fig. S6), Ga-doped Ag NCs are, in part, transformed into hexagonal close-packed (hcp) Ag_3Ga NCs and the Ga islands on the NC surfaces have merged, forming a shell structure. The delay in conversion to the Ag_3Ga phase (10-min aliquot; Fig. 2F) can be partially attributed to diffusion kinetics and a miscibility gap (3 to 10 atomic %) between the fcc and hcp phases (fig. S7). Considering our synthesis of other IMC materials (Fig. 1), we hypothesize that this mechanism, based on accumulation of amalgamating metal on the NC surface, fast diffusion of these low–melting point metals (Ga, In, and Zn), and stepwise conversion to intermetallic phases, is generalizable.

Composition control

The amalgamation seeded growth method offers easy and quantitative control over the resulting NC compositions. The amount of amalgamating metal precursor determines the stoichiometry of the resulting IMC NCs, as highlighted for the Au-Ga system (Fig. 3). In case of Au-Ga, small amounts of introduced Ga-amide result in fcc Ga-doped Au NCs, while proportionally larger quantities of Ga precursor lead to the conversion of Au seeds to various intermetallic phases including hexagonal Au_7Ga_2, orthorhombic AuGa, and cubic $AuGa_2$. All IMC NCs are characterized by high phase purity (figs. S3D, S8, and S9) and narrow size distributions (Figs. 1E and 3, B to D, and table S1). In analogy to fcc Ga-doped Au NCs, plasmonic fcc Ga-doped Ag and fcc Ga-doped Cu NCs are prepared by decreasing the amount of Ga precursor proportionally (fig. S10 and S11). By selecting an amount of Ga precursor in between amounts yielding single-phase IMC NCs, we obtain a quantitative mixture of two phases (Fig. 3A and figs. S12 to S14). STEM EDX maps show that in these mixed phase samples, the two intermetallic phases occur on different particles rather than within the same particle. This observation further supports the proposed amalgamation mechanism of stepwise conversion to Ga-enriched IMC NCs, because each individual NC is compositionally uniform (fig. S13) and the amount of amalgamating metal disposed on the seeds solely determines the final phase composition (Fig. 3A).

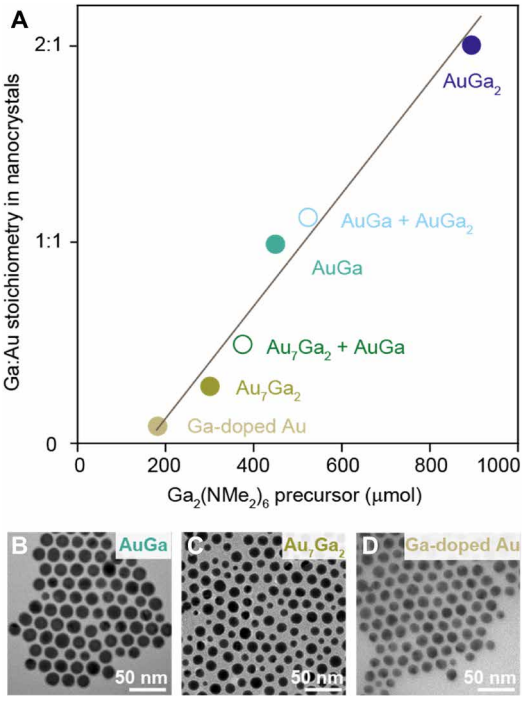

Fig. 3. Composition control. (**A**) Ratio between the constituent metals of IMC NCs in relation to the amount of introduced amalgamation metal precursor, as shown for the Au-Ga system. (**B** to **D**) As-synthesized AuGa, Au_7Ga_2, and Ga-doped Au NCs are shown in TEM images.

Size control

Furthermore, amalgamation seeded growth enables excellent control over the size and size uniformity of IMC NCs. We highlight this for a size series of $AuGa_2$ NCs obtained via amalgamation of Au seeds of various sizes (Fig. 4, A to G, and fig. S15). We predict the diameter of IMC NCs from an expected volume expansion upon alloying, calculated from the diameter of the metal seeds and the ratio of the seed metal and intermetallic phase densities according to Eq. 3. We find a good agreement with the obtained sizes for all IMC NCs (Fig. 4A and fig. S16). In addition, we demonstrate the preservation of size uniformity upon amalgamation by comparing the size distributions of IMC NCs (Ag_3Ga, Cu_2Ga, Ni_2Ga_3, $AuGa_2$, and PdGa) and the initial seeds (Fig. 4H). Thus, highly monodisperse IMC NCs can be obtained when metal seeds with narrow size distributions are used in the synthesis (e.g., 5.4% for Ni_2Ga_3 NCs; Fig. 4H).

DISCUSSION

We have developed the amalgamation seeded growth as a generalizable synthetic approach to achieve monodisperse intermetallic NCs (IMC NCs) with size and composition control. The synthesis is predictive and quantitative: The amount of amalgamating metal defines the stoichiometry and phase purity of the resulting IMC NCs, and the size and size distribution of the seed NCs determine their diameter and size uniformity. Other seeded growth routes for bimetallic NCs include epitaxial seeded growth (*35*) and galvanic exchange reactions (*39*, *40*). Specific bimetallic compositions have been reported for both routes, e.g., coinage metal alloys (*41*) and Sn-based alloys (*42*). In comparison, amalgamation seeded growth synthesis emerges as a versatile and atom-economic method for highly uniform IMC NCs, because it is not limited by epitaxial constraints or relying on the occurrence of redox reactivity between template seeds and a second metal.

In conclusion, we demonstrate the synthesis of crystalline and compositionally uniform intermetallic colloids of various compositions through amalgamation of different metal seeds (Au, Ag, Cu, Pd, and Ni) with low–melting point metals (Ga, In, and Zn) and obtain stable dispersions under ambient conditions, which are easy to handle and process. Considering the large family of low–melting point metals (fig. S17) and the ever increasing number of reports on

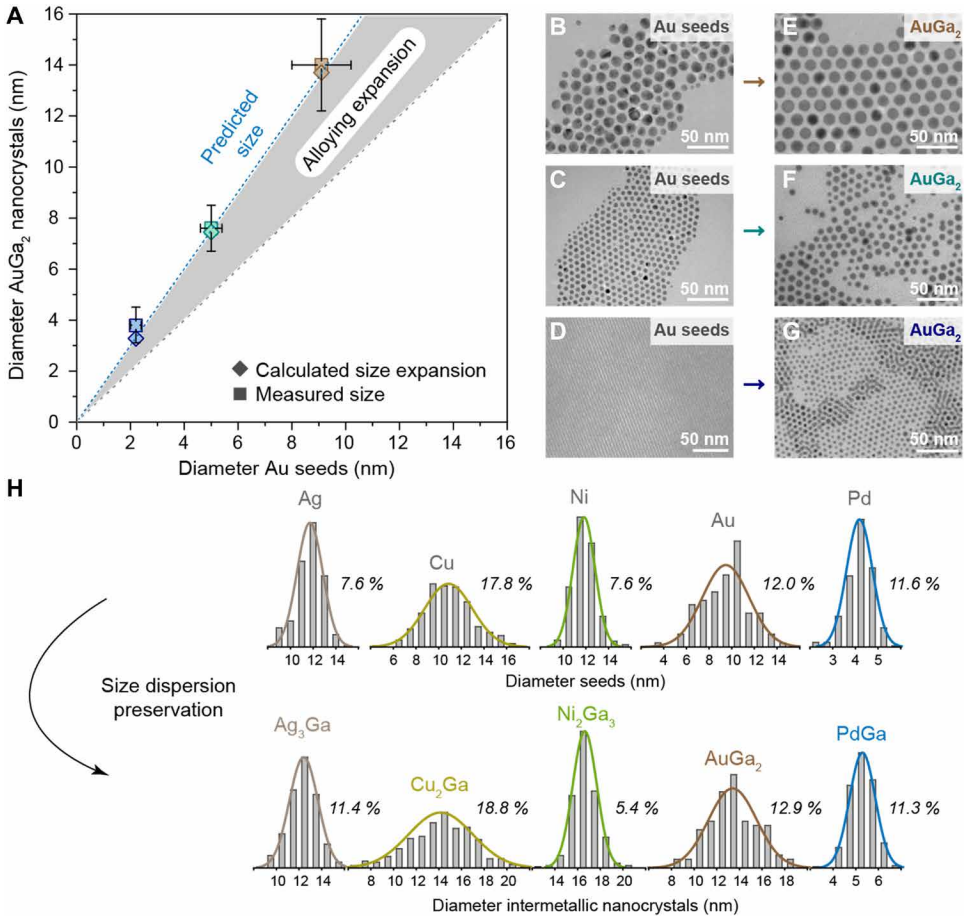

Fig. 4. Size control. Experimentally obtained and calculated diameters of $AuGa_2$ NCs, as prepared from various sizes of initial Au seeds (**A**) and corresponding TEM images (**B** to **G**). The shaded area in (A) illustrates the increase of NC size upon amalgamation reaction (note a good agreement between predicted and measured size of $AuGa_2$ NCs). (**H**) A comparison between size distribution histograms of initial seeds (Ag, Cu, Ni, Au, and Pd) and corresponding IMC NCs (Ag_3Ga, Cu_2Ga, Ni_2Ga_3, $AuGa_2$, and PdGa) reveals the preservation of size dispersion characteristics (polydispersity percentages are given next to histograms) upon amalgamation.

monometallic and alloy NCs, we envision that amalgamation seeded growth can be used to achieve nanocrystals of numerous other IMCs of interest for the many applications considered for these materials.

MATERIALS AND METHODS

Experimental design

The Amalgamation seeded growth method involves the reaction between monometallic seed NCs (Au, Ag, Cu, Pd, or Ni) and amides of a second, low–melting point metal (Ga, In, or Zn). We report complete synthesis descriptions for many bimetallic NCs (e.g., Pd-containing compositions below and other bimetallic NCs in the Supplementary Materials), reveal the mechanism of reaction, and provide details for comprehensive structural and optical characterization of obtained IMC NCs.

Synthesis of PdGa, PdIn, and PdZn NCs

Pd seeds (4.3 ± 0.5 nm) were synthesized according to a previously reported procedure (*43*). A yellow-colored Pd-precursor solution was prepared by dissolving 50 mg (0.164 mmol) of $Pd(acac)_2$ in 5 ml of oleylamine and 0.5 ml of trioctylphosphine inside the glovebox. The Pd-precursor solution was then transferred to an evacuated three-neck flask. Next, the solution was brought to a temperature of 250°C for 30 min under N_2 flow, during which the synthesis solution turned into a gray-colored dispersion of Pd seeds. The synthesis solution of Pd seeds was then cooled down to room temperature, evacuated for 10 min to remove volatile by-products resulting from the seed synthesis, and brought back to 260°C under N_2 flow. This was followed by the swift injection of an amalgamating metal precursor solution, prepared by dissolving either 300 mg (0.74 mmol) of $Ga_2(NMe_2)_6$ or 300 mg (0.50 mmol) of $In[N(SiMe_3)_2]_3$ in squalane (3 ml) or by measuring 0.1 ml (0.25 mmol) of $Zn[N(SiMe_3)_2]_2$. The synthesis was brought to a temperature of 280°C for 10 min, and the reaction was subsequently terminated by cooling down to room temperature. To purify the synthesis solution, NCs were precipitated with 50 ml of ethanol, followed by centrifugation for 5 min at 6000 rpm. The NCs were subsequently redispersed in hexane (5 ml) and oleic acid (0.5 ml), and this precipitation/redispersion cycle was repeated two more times. Last, the resulting NCs were dispersed in hexane (5 ml) and stored under ambient conditions.

Electron microscopy measurements

TEM images were captured with a Hitachi HT7700 microscope operating at 100 kV. High-angle annular dark-field scanning TEM

(STEM) images, STEM EDX elemental maps, and HRTEM images were collected with an FEI Talos microscope operating at 200 kV. Aberration-corrected HRSTEM images were taken with a Hitachi HD2700 microscope operating at 200 kV. To prepare the NC monolayers, diluted colloidal dispersions of NCs in hexane were drop-cast onto a carbon grid. Size distribution analysis was performed by counting the diameters of 300 NCs in the acquired TEM images using ImageJ software, neglecting oxide shells. Size deviations were obtained from Eq 1, using a Gaussian fit of the obtained size histograms

$$s = \frac{\text{fwhm}}{2} \quad (1)$$

where fwhm is the full width at half maximum of the Gaussian fit.

Powder XRD measurements

Powder XRD patterns were measured on the Rigaku SmartLab 9 kW System, equipped with a rotating Cu anode and a two-dimensional solid-state detector (HyPix-3000 SL). Colloidal solutions were drop-casted on a high-hkl cut Si substrate and measured in parallel beam geometry (a step size of 0.05° and a scanning speed of 0.7°/min were used). Rietveld refinements were performed using FullProf Suite software. Crystallite sizes were calculated from the Scherrer equation (*44*), Eq. 2, using a Gaussian fit of three diffraction peaks per collected XRD pattern and providing an average crystallite size value

$$\tau = \frac{K\lambda}{\beta\cos\theta} \quad (2)$$

where τ is the mean size of the crystalline domains, K is a dimensionless shape factor with a chosen value of 0.9, λ is the x-ray wavelength (0.15406 nm), β is the line broadening at full width at half maximum of the Gaussian fit after subtracting the instrumental line broadening, and θ is the Bragg angle.

UV-Vis extinction measurements

Ultraviolet-visible (UV-Vis) extinction spectra were acquired with an Agilent Cary 5000 spectrophotometer. NC dispersions in hexane were put in a quartz cuvette and referenced with a blank solvent.

Size expansion calculations

The size expansion of metal seeds upon alloying into intermetallic NCs was calculated from Eq. 3

$$d_2 = d_1\sqrt[3]{\frac{\rho_1}{\rho_2 * w_1}} \quad (3)$$

where d_2 is the diameter of the resulting intermetallic NCs, d_1 is the diameter of the metal seeds, ρ_2 is the density of intermetallic phase, ρ_1 is the density of seed metal, and w_1 is the mass fraction of the seed metal in the IMC. This formula is derived from the mass of the seeds, which is the mass of the IMC NCs factorized with the weight fraction of the seed metal in the intermetallic phase.

SUPPLEMENTARY MATERIALS

Supplementary material for this article is available at http://advances.sciencemag.org/cgi/content/full/7/31/eabg1934/DC1

REFERENCES AND NOTES

1. D. V. Talapin, J.-S. Lee, M. V. Kovalenko, E. V. Shevchenko, Prospects of colloidal nanocrystals for electronic and optoelectronic applications. *Chem. Rev.* **110**, 389–458 (2010).
2. M. Zhong, K. Tran, Y. Min, C. Wang, Z. Wang, C.-T. Dinh, P. De Luna, Z. Yu, A. S. Rasouli, P. Brodersen, S. Sun, O. Voznyy, C.-S. Tan, M. Askerka, F. Che, M. Liu, A. Seifitokaldani, Y. Pang, S.-C. Lo, A. Ip, Z. Ulissi, E. H. Sargent, Accelerated discovery of CO_2 electrocatalysts using active machine learning. *Nature* **581**, 178–183 (2020).
3. Y. C. Yan, J. S. Du, K. D. Gilroy, D. Yang, Y. Xia, H. Zhang, Intermetallic nanocrystals: Syntheses and catalytic applications. *Adv. Mater.* **29**, 1605997 (2017).
4. S. Furukawa, T. Komatsu, Intermetallic compounds: Promising inorganic materials for well-structured and electronically modified reaction environments for efficient catalysis. *ACS Catal.* **7**, 735–765 (2017).
5. D. S. Wang, Y. D. Li, Bimetallic nanocrystals: Liquid-phase synthesis and catalytic applications. *Adv. Mater.* **23**, 1044–1060 (2011).
6. S. Yazdani, M. T. Pettes, Nanoscale self-assembly of thermoelectric materials: A review of chemistry-based approaches. *Nanotechnology* **29**, 432001 (2018).
7. B. Poudel, Q. Hao, Y. Ma, Y. Lan, A. Minnich, B. Yu, X. Yan, D. Wang, A. Muto, D. Vashaee, X. Chen, J. Liu, M. S. Dresselhaus, G. Chen, Z. Ren, High-thermoelectric performance of nanostructured bismuth antimony telluride bulk alloys. *Science* **320**, 634–638 (2008).
8. P. H. Yeh, L. J. Chen, P. T. Liu, D. Y. Wang, T. C. Chang, Metal nanocrystals as charge storage nodes for nonvolatile memory devices. *Electrochim. Acta* **52**, 2920–2926 (2007).
9. N. Jeong, J. G. Yeo, Selective synthesis and superconductivity of In-Sn intermetallic nanowires sheathed in carbon nanotubes. *Nanotechnology* **23**, 285604 (2012).
10. L. Li, Y. Zheng, S. Zhang, J. Yang, Z. Shao, Z. Guo, Recent progress on sodium ion batteries: Potential high-performance anodes. *Energ. Environ. Sci.* **11**, 2310–2340 (2018).
11. M. K. Debe, Electrocatalyst approaches and challenges for automotive fuel cells. *Nature* **486**, 43–51 (2012).
12. M. Luo, Y. Sun, L. Wang, S. Guo, Tuning multimetallic ordered intermetallic nanocrystals for efficient energy electrocatalysis. *Adv. Energy Mater.* **7**, 1602073 (2017).
13. M. Zhou, C. Li, J. Fang, Noble-metal based random alloy and intermetallic nanocrystals: Syntheses and applications. *Chem. Rev.* **121**, 736–795 (2021).
14. L. Dong, Y. Liu, Y. Lu, L. Zhang, N. Man, L. Cao, K. Ma, D. An, J. Lin, Y.-J. Xu, W.-P. Xu, W.-B. Wu, S.-H. Yu, L.-P. Wen, Tuning magnetic property and autophagic response for self-assembled Ni-Co alloy nanocrystals. *Adv. Funct. Mater.* **23**, 5930–5940 (2013).
15. S. Sun, C. B. Murray, D. Weller, L. Folks, A. Moser, Monodisperse FePt nanoparticles and ferromagnetic FePt nanocrystal superlattices. *Science* **287**, 1989–1992 (2000).
16. H. You, S. Yang, B. Ding, H. Yang, Synthesis of colloidal metal and metal alloy nanoparticles for electrochemical energy applications. *Chem. Soc. Rev.* **42**, 2880–2904 (2013).
17. F. Studt, I. Sharafutdinov, F. Abild-Pedersen, C. F. Elkjær, J. S. Hummelshøj, S. Dahl, I. Chorkendorff, J. K. Nørskov, Discovery of a Ni-Ga catalyst for carbon dioxide reduction to methanol. *Nat. Chem.* **6**, 320–324 (2014).
18. F. Studt, F. Abild-Pedersen, T. Bligaard, R. Z. Sørensen, C. H. Christensen, J. K. Nørskov, Identification of non-precious metal alloy catalysts for selective hydrogenation of acetylene. *Science* **320**, 1320–1322 (2008).
19. A. Han, J. Zhang, W. Sun, W. Chen, S. Zhang, Y. Han, Q. Feng, L. Zheng, L. Gu, C. Chen, Q. Peng, D. Wang, Y. Li, Isolating contiguous Pt atoms and forming Pt-Zn intermetallic nanoparticles to regulate selectivity in 4-nitrophenylacetylene hydrogenation. *Nat. Commun.* **10**, 3787 (2019).
20. Y. Hu, J. O. Jensen, L. N. Cleemann, B. A. Brandes, Q. Li, Synthesis of Pt-rare earth metal nanoalloys. *J. Am. Chem. Soc.* **142**, 953–961 (2020).
21. Y. Hu, Y. Lu, X. Zhao, T. Shen, T. Zhao, M. Gong, K. Chen, C. Lai, J. Zhang, H. L. Xin, D. Wang, Highly active N-doped carbon encapsulated Pd-Fe intermetallic nanoparticles for the oxygen reduction reaction. *Nano Res.* **13**, 2365–2370 (2020).
22. J. S. Kanady, P. Leidinger, A. Haas, S. Titlbach, S. Schunk, K. Schierle-Arndt, E. J. Crumlin, C. H. Wu, A. P. Alivisatos, Synthesis of Pt_3Y and other early-late intermetallic nanoparticles by way of a molten reducing agent. *J. Am. Chem. Soc.* **139**, 5672–5675 (2017).
23. M. V. Kovalenko, L. Manna, A. Cabot, Z. Hens, D. V. Talapin, C. R. Kagan, V. I. Klimov, A. L. Rogach, P. Reiss, D. J. Milliron, P. Guyot-Sionnnest, G. Konstantatos, W. J. Parak, T. Hyeon, B. A. Korgel, C. B. Murray, W. Heiss, Prospects of nanoscience with nanocrystals. *ACS Nano* **9**, 1012–1057 (2015).
24. R. E. Cable, R. E. Schaak, Solution synthesis of nanocrystalline M-Zn (M = Pd, Au, Cu) intermetallic compounds via chemical conversion of metal nanoparticle precursors. *Chem. Mater.* **19**, 4098–4104 (2007).
25. T. R. Gordon, R. E. Schaak, Synthesis of hybrid Au-In_2O_3 nanoparticles exhibiting dual plasmonic resonance. *Chem. Mater.* **26**, 5900–5904 (2014).
26. M. Armbrüster, G. Wowsnick, M. Friedrich, M. Heggen, R. Cardoso-Gil, Synthesis and catalytic properties of nanoparticulate intermetallic Ga-Pd compounds. *J. Am. Chem. Soc.* **133**, 9112–9118 (2011).
27. S. Jana, J. W. Chang, R. M. Rioux, Synthesis and modeling of hollow intermetallic Ni-Zn nanoparticles formed by the Kirkendall effect. *Nano Lett.* **13**, 3618–3625 (2013).
28. W. Chen, R. Yu, L. Li, A. Wang, Q. Peng, Y. Li, A seed-based diffusion route to monodisperse intermetallic CuAu nanocrystals. *Angew. Chem. Int. Ed.* **49**, 2917–2921 (2010).
29. G. Bjørklund, "The history of dental amalgam" in *Tidsskr. Nor. Laegeforen* **109**, 3582–3585 (1989).

30. M. Yarema, R. Caputo, M. V. Kovalenko, Precision synthesis of colloidal inorganic nanocrystals using metal and metalloid amides. *Nanoscale* **5**, 8398–8410 (2013).
31. S. Mourdikoudis, L. M. Liz-Marzán, Oleylamine in nanoparticle synthesis. *Chem. Mater.* **25**, 1465–1476 (2013).
32. Y. Yu, W. Yang, X. Sun, W. Zhu, X.-Z. Li, D. J. Sellmyer, S. Sun, Monodisperse MPt (M = Fe, Co, Ni, Cu, Zn) nanoparticles prepared from a facile oleylamine reduction of metal salts. *Nano Lett.* **14**, 2778–2782 (2014).
33. Y. Yin, C. K. Erdonmez, A. Cabot, S. Hughes, A. P. Alivisatos, Colloidal synthesis of hollow cobalt sulfide nanocrystals. *Adv. Funct. Mater.* **16**, 1389–1399 (2006).
34. J. Huang, Y. Yan, X. Li, X. Qiao, X. Wu, J. Li, R. Shen, D. Yang, H. Zhang, Unexpected Kirkendall effect in twinned icosahedral nanocrystals driven by strain gradient. *Nano Res.* **13**, 2641–2649 (2020).
35. S. E. Habas, H. Lee, V. Radmilovic, G. A. Somorjai, P. Yang, Shaping binary metal nanocrystals through epitaxial seeded growth. *Nat. Mater.* **6**, 692–697 (2007).
36. H. Yu, P. C. Gibbons, K. F. Kelton, W. E. Buhro, Heterogeneous seeded growth: A potentially general synthesis of monodisperse metallic nanoparticles. *J. Am. Chem. Soc.* **123**, 9198–9199 (2001).
37. Y. Liu, Z. Zhu, G. Liu, Z. Xu, S. M. Kuznicki, H. Zhang, A novel method to improve crystallinity of supported nanoparticles using low melting point metals. *J. Phys. Chem. C* **115**, 14591–14597 (2011).
38. K. Arakawa, K. Yamamoto, K. Sakai, H. Koizumi, Transitory embrittlement of polycrystalline silver by liquid gallium. *Mater. Trans.* **55**, 653–657 (2014).
39. X. Lu, H.-Y. Tuan, J. Chen, Z.-Y. Li, B. A. Korgel, Y. Xia, Mechanistic studies on the galvanic replacement reaction between multiply twinned particles of Ag and $HAuCl_4$ in an organic medium. *J. Am. Chem. Soc.* **129**, 1733–1742 (2007).
40. D. Kriegner, M. Sytnyk, H. Groiss, M. Yarema, W. Grafeneder, P. Walter, A.-C. Dippel, M. Meffert, D. Gerthsen, J. Stangl, W. Heiss, Galvanic exchange in colloidal metal/metal-oxide core/shell nanocrystals. *J. Phys. Chem. C* **120**, 19848–19855 (2016).
41. Z. Niu, S. Chen, Y. Yu, T. Lei, A. Dehestani, K. Schierle-Arndt, P. Yang, Morphology-controlled transformation of Cu@Au core-shell nanowires into thermally stable Cu_3Au intermetallic nanowires. *Nano Res.* **13**, 2564–2569 (2020).
42. N. H. Chou, R. E. Schaak, Shape-controlled conversion of β-Sn nanocrystals into intermetallic M-Sn (M = Fe, Co, Ni, Pd) nanocrystals. *J. Am. Chem. Soc.* **129**, 7339–7345 (2007).
43. S.-W. Kim, J. Park, Y. Jang, Y. Chung, S. Hwang, T. Hyeon, Y. W. Kim, Synthesis of monodisperse palladium nanoparticles. *Nano Lett.* **3**, 1289–1291 (2003).
44. A. L. Patterson, The Scherrer formula for x-ray particle size determination. *Phys. Rev.* **56**, 978–982 (1939).
45. E. Dhaene, J. Billet, E. Bennett, I. Van Driessche, J. De Roo, The trouble with ODE: Polymerization during nanocrystal synthesis. *Nano Lett.* **19**, 7411–7417 (2019).
46. H. Bürger, J. Cichon, U. Goetze, U. Wannagat, H. J. Wismar, Chemistry of silicon-nitrogen compounds: Synthesis, vibrational spectra, and normal coordinate analysis of disilylamides of group III $M[N(SiMe_3)_2]_3$ with M = Al, Ga, and In. *J. Organomet. Chem.* **33**, 1–12 (1971).
47. H. Hiramatsu, F. E. Osterloh, A simple large-scale synthesis of nearly monodisperse gold and silver nanoparticles with adjustable sizes and with exchangeable surfactants. *Chem. Mater.* **16**, 2509–2511 (2004).
48. S. Peng, Y. Lee, C. Wang, H. Yin, S. Dai, S. Sun, A facile synthesis of monodisperse Au nanoparticles and their catalysis of CO oxidation. *Nano Res.* **1**, 229–234 (2008).
49. S. Peng, J. M. McMahon, G. C. Schatz, S. K. Gray, Y. G. Sun, Reversing the size-dependence of surface plasmon resonances. *Proc. Natl. Acad. Sci. U.S.A.* **107**, 14530–14534 (2010).
50. A. Loiudice, P. Lobaccaro, E. A. Kamali, T. Thao, B. H. Huang, J. W. Ager, R. Buonsanti, Tailoring copper nanocrystals towards C_2 products in electrochemical CO_2 reduction. *Angew. Chem. Int. Ed.* **55**, 5789–5792 (2016).
51. S. Carenco, C. Boissière, L. Nicole, C. Sanchez, P. Le Floch, N. Mézailles, Controlled design of size-tunable monodisperse nickel nanoparticles. *Chem. Mater.* **22**, 1340–1349 (2010).
52. M. Yarema, M. Wörle, M. D. Rossell, R. Erni, R. Caputo, L. Protesescu, K. V. Kravchyk, D. N. Dirin, K. Lienau, F. von Rohr, A. Schilling, M. Nachtegaal, M. V. Kovalenko, Monodisperse colloidal gallium nanoparticles: Synthesis, low temperature crystallization, surface plasmon resonance and Li-ion storage. *J. Am. Chem. Soc.* **136**, 12422–12430 (2014).
53. M. R. Baren, The Ag-Ga (silver-gallium) system. *Bull. Alloy Phase Diagrams* **11**, 334–339 (1990).
54. S. Liu, Z. Sun, Q. Liu, L. Wu, Y. Huang, T. Yao, J. Zhang, T. Hu, M. Ge, F. Hu, Z. Xie, G. Pan, S. Wei, Unidirectional thermal diffusion in bimetallic Cu@Au nanoparticles. *ACS Nano* **8**, 1886–1892 (2014).
55. H. A. Atwater, A. Polman, Plasmonics for improved photovoltaic devices. *Nat. Mater.* **9**, 205–213 (2010).
56. J. F. Li, Y. F. Huang, Y. Ding, Z. L. Yang, S. B. Li, X. S. Zhou, F. R. Fan, W. Zhang, Z. Y. Zhou, D. Y. Wu, B. Ren, Z. L. Wang, Z. Q. Tian, Shell-isolated nanoparticle-enhanced Raman spectroscopy. *Nature* **464**, 392–395 (2010).
57. J.-F. Li, Y.-J. Zhang, S.-Y. Ding, R. Panneerselvam, Z.-Q. Tian, Core-shell nanoparticle-enhanced Raman spectroscopy. *Chem. Rev.* **117**, 5002–5069 (2017).
58. Z. Wang, Z. Chen, H. Zhang, Z. Zhang, H. Wu, M. Jin, C. Wu, D. Yang, Y. Yin, Lattice-mismatch-induced twinning for seeded growth of anisotropic nanostructures. *ACS Nano* **9**, 3307–3313 (2015).
59. S. Jeong, Y. Liu, Y. Zhong, X. Zhan, Y. Li, Y. Wang, P. M. Cha, J. Chen, X. Ye, Heterometallic seed-mediated growth of monodisperse colloidal copper nanorods with widely tunable plasmonic resonances. *Nano Lett.* **20**, 7263–7271 (2020).

Acknowledgments: We thank A. Landuyt and J.-M. Sujata for topical and intellectual discussions and M. Mücklich for technical assistance. Electron microscopy measurements were performed at the Scientific Center for Optical and Electron Microscopy (ScopeM) of the Swiss Federal Institute of Technology. **Funding:** This study was supported by Swiss National Science Foundation Ambizione Fellowship, grant 161249; Eidgenössische Technische Hochschule Zürich, ETH Zürich, ETH Research Grant (ETH-37 18-2); and European Research Council (ERC) under the European Union's Horizon 2020 research and innovation programme, grant agreement no. 852751. **Author contributions:** Conceptualization: J.C. and M.Y.; methodology: J.C. and M.Y.; investigation: J.C., A.M., O.Y., and M.Y.; visualization: J.C. and M.Y.; supervision: M.Y. and V.W.; writing—original draft: J.C.; writing—review and editing: J.C., M.Y., and V.W. **Competing interests:** The authors declare that they have no competing interests. **Data and materials availability:** All data needed to evaluate the conclusions in the paper are present in the paper and/or the Supplementary Materials.

Submitted 16 December 2020
Accepted 11 June 2021
Published 28 July 2021
10.1126/sciadv.abg1934

Citation: J. Clarysse, A. Moser, O. Yarema, V. Wood, M. Yarema, Size- and composition-controlled intermetallic nanocrystals via amalgamation seeded growth. *Sci. Adv.* **7**, eabg1934 (2021).